RSC Advances

PAPER

View Article Online
View Journal | View Issue

Cite this: *RSC Adv.*, 2022, **12**, 3386

Tunable giant magnetoresistance ratio in bilayer CuPc molecular devices

Jianhua Liu, †[ab] Kun Luo,†[ab] Hudong Chang,[ab] Bing Sun,[ab] Shengli Zhang *[c] and Zhenhua Wu *[ab]

We investigate the influence of the distance between the buffer layer and the central molecule on the electrical transport, spin-filter transport, magnetoresistance effects and thermoelectric properties of a bilayer CuPc molecular device with V-shaped zigzag-edged graphene nanoribbon (VZGNR) electrodes by combining density functional theory and the non-equilibrium Green's function. The results show that the spin-dependent total conductance and spin filter efficiency of the bilayer CuPc molecular device reach a maximum with a parallel spin configuration (PC) when the carbon atom at the edge of the electrode is in the center of the carbon atom at the edge of the bilayer molecules due to the stronger coupling interaction between the double-layer molecules and the leads. Moreover, the spin polarization of the bilayer CuPc molecular device is reversed at certain distances; there is a minimum spin filter efficiency (SFE) of −99.93448% and a maximum SFE of 97.91% observed in the anti-parallel spin configuration (APC) of the device and there is a minimum SFE of −26.03175% and a maximum SFE of 99.99996% observed with the PC at zero bias. The SFE oscillates with increasing considered bias voltage in the PC and APC when the distances are $d = 0$ Å and $d = -1.06$ Å, and a negative differential resistance (NDR) effect was observed. For the PC and APC, there is a giant magnetoresistance (MR) effect and the MR ratio exceeds 5.21×10^7% (99.9996%), and the MR ratio oscillates with increasing considered bias voltage when $d = 0$ Å. The MR ratio could be reserved by applying a certain bias voltage. These transport behaviors can be well understood by analyzing the transmission spectra, projected density of states and scattering states. There are pure spin Seebeck coefficients and pure charge Seebeck coefficients at certain temperatures when the distances are certain values, which means that the corresponding temperature differences could produce pure spin current and pure charge current, respectively. Our results provide new ideas for designing ultrahigh-performance spintronic molecular devices.

Received 3rd October 2021
Accepted 8th January 2022

DOI: 10.1039/d1ra07360e

rsc.li/rsc-advances

1. Introduction

Molecular spintronics is a promising approach in downsizing spintronic devices, storing high-density data and quantum computing[1,2] to achieve the negative differential resistance (NDR) effect,[3] spin filtering effect[4] and giant magnetoresistance (GMR) effect[5] studied in molecular spintronic devices. One of the important characteristics of molecular spintronic devices is that they are able to generate a large spin-filter efficiency (SFE) by adopting a magnetic molecule sandwiched between the two nonmagnetic electrodes.[6–8] The SFE in FePc with gold electrodes can be prominently affected by tuning carbon chains with different connection positions.[9] A study of matching styles between CuPc and the electrode indicated that a symmetrical matching interaction will enhance electron transport.[10] Injecting holes into the molecular orbitals or resonance electrons of the SnPc molecule can realize the conversion between spin-up filtering and spin-down filtering.[11,12] Single-molecule magnets can be connected to gold electrodes through sulfur atoms[13,14] and connected to carbon nanotube electrodes or graphene nanoribbon electrodes through carbon atoms.[15,16] Different magnetic structures cause a resistance change, which could be quantitatively described by the MR ratio.[17] MR ratios of 27% and $\sim 2 \times 10^7$% were found in a Ni-bezenedithiol-Ni molecular junction[18] and ZGNR-based molecular junctions,[19] respectively. The spin-dependent hybridization of the electrode and molecular orbitals could cause a large MR.[5] Perfect SFE and GMR effects were observed in an MnPc molecular device.[17] Bipolar SFE, NDR and spin rectifying effect were found in an all-carbon multifunctional spintronic device.[20] Metal (Co, Cr, Fe and Mo)-

[a]*Institute of Microelectronics of Chinese Academy of Sciences, Beijing 100029, China. E-mail: wuzhenhua@ime.ac.cn*

[b]*College of Microelectronics, University of Chinese Academy of Sciences, Beijing 100029, China*

[c]*MIIT Key Laboratory of Advanced Display Materials and Devices, School of Materials Science and Engineering, Nanjing University of Science and Technology, Nanjing 210094, China. E-mail: zhangslvip@njust.edu.cn*

† These authors contributed equally.

salophen molecular chains exhibited almost ideal SFE, and there was a GMR of over 10^9 for the Co-salophen molecular chain.[21] In our previous work, we investigated the quantum transport properties of a twisted bilayer CuPc molecular device and found that the twist angle could effectively modulate the conductance and SFE of the CuPc molecular device.[22] For a topological insulator quantum dot, its conductance could be adjusted by changing the quantum well bandgap, the width of the topological insulator constrictions and the Fermi energy.[23]

In this paper, we studied the spin transport and thermoelectric properties of a bilayer CuPc molecular device with two VZGNR electrodes by non-equilibrium Green's function in combination with density functional theory[24,25] for two conditions: a parallel spin configuration (PC) and an anti-parallel spin configuration (APC). We found that bilayer CuPc molecular devices show ultrahigh spin filter efficiency at zero bias when the distances between the buffer layer and CuPc molecule are certain values, which exceed 99.99996% and 97.91% for PC and APC, respectively. Meanwhile, we observed that the SFE decreases and the spin-polarized current shows an increasing trend with a bias for the PC. Interestingly, the spin polarization of the bilayer CuPc molecular device could be reversed when the distance was a certain value and the MR could also be reserved by applying a specific bias voltage. Particularly, there are reserved SFEs for PC and APC when the distances are certain values and the reserved SFEs exceed −26.03175% and −99.93448%, respectively. The MR ratio exceeds 5.21×10^7% (99.9996%). When the distances are at certain values, there are pure spin Seebeck coefficients and pure charge Seebeck coefficients at certain temperatures.

2. Computational details

We investigated the spin transport properties of a bilayer CuPc molecular device with different distances between the buffer layer linked with the lead and the central position of the atoms at the edge of the bilayer CuPc molecules by combining density functional theory and the non-equilibrium Green's function approach, as implemented by the Nanodcal transport package.[26] The device is formed by three parts: right and left electrodes (which extend to $\pm\infty$) and a central scattering region, which contains two CuPc molecules, as well as left and right buffer layers. The energy cutoff is set to 150 Rydberg, the k-point grid is chosen to be $100 \times 1 \times 1$ and the electrode temperature is set to 300 K. We introduced a vacuum layer of about 15 Å in the y and z directions to eliminate interaction between GNRs in neighboring cells and the edge atoms, both electrodes and the central region are saturated with hydrogen atoms to remove dangling bonds.[22,27] The exchange–correlation function is described by the local density approximation proposed by Perdew and Zunger. We defined the distance as zero when the edge atoms of the buffer layer linked with the lead are at the central position of the atoms at the adjacent edge of the bilayer CuPc molecules, as shown in Fig. 1. When the buffer layer is kept away from the two CuPc molecules, the distance is positive; otherwise, it is negative. The quantum transport phenomena with the bilayer CuPc molecular device are further understood by analyzing the transmission spectrum, density of states and the scattering states.

The spin-polarized current through the central scattering region is calculated by the Landauer–Buttiker formula as follows[28]

$$I_\sigma(V_b) = \frac{e}{h}\int T_\sigma(\varepsilon,\ V_b)[f(\varepsilon-\mu_L) - f(\varepsilon-\mu_R)]d\varepsilon \quad (1)$$

where e is the electron charge, h is Planck's constant, $T_\sigma(\varepsilon, V_b)$ is the electron transmission coefficient for the spin-up (↑) and spin-down (↓) electrons ($\sigma = \uparrow/\downarrow$), $f(\varepsilon - \mu_{L/R})$ is the Fermi distribution function, and μ_L and μ_R represent the electrochemical potentials of the left and right electrode, respectively. V_b is the bias voltage and I_σ is the total charge current. For every spin state, $T_\sigma(\varepsilon, V)$ is given by[17,28]

$$T_\sigma(\varepsilon,\ V_b) = \mathrm{Tr}[\Gamma_L(\varepsilon,\ V_b)G^R(\varepsilon)\Gamma_R(\varepsilon,\ V_b)G^A(\varepsilon)] \quad (2)$$

The spin-polarized conductance at zero bias is given by the Landauer–Buttiker formula[28] and is derived from the current with respect to the voltage,[29] as follows

$$G_\sigma = \frac{e^2}{h}T_\sigma(E_F) \quad (3)$$

where E_F is the Fermi level. The spin-polarized conductance unit is $G_0 = e^2/h$. For each spin state, $T_\sigma(E_F)$ is given by[17]

$$T_\sigma(E_F) = \mathrm{Tr}[\Gamma_L G^R \Gamma_R G^A]_{\sigma\sigma} \quad (4)$$

where Γ_L and Γ_R represent the contact broadening functions associated with the left and right electrode, and G^R and G^A stand for the retarded and advanced Green's functions of the central region, respectively.

At zero bias, SFE is defined as

$$\mathrm{SFE} = \frac{T_\downarrow(E_F) - T_\uparrow(E_F)}{T_\uparrow(E_F) + T_\downarrow(E_F)} \times 100\% \quad (5)$$

where $T_\uparrow(E_F)$ and $T_\downarrow(E_F)$ stand for the transmission coefficient of the spin-up (SU) and spin-down (SD) states at the Fermi level, respectively.

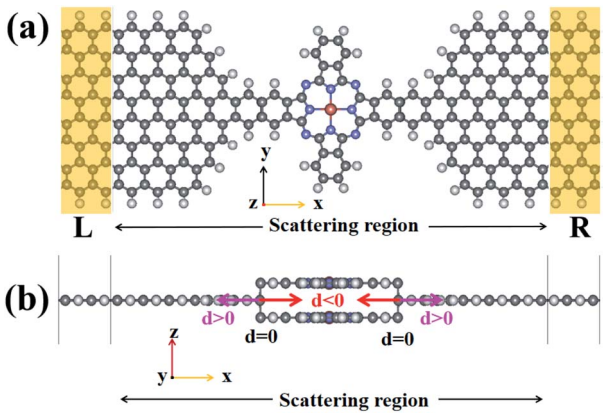

Fig. 1 The structure of the bilayer CuPc molecular device. The red, blue, black, and grey balls represent Cu, N, C, and H atoms, respectively. The molecule in the scattering region is CuPc and the electrode is a V-shaped zigzag-edged GNR electrode. (a) and (b) are the top and side view of the molecular device, respectively.

Considering the spin direction of the lead, there is a giant magnetoresistance (MR) effect, and the MR ratios for the device for PC and APC are defined by the following two formulae[20]

$$\mathrm{MR1} = \frac{T_{\mathrm{PC}} - T_{\mathrm{APC}}}{T_{\mathrm{APC}}} \times 100\% \quad (6)$$

$$\mathrm{MR2} = \frac{T_{\mathrm{PC}} - T_{\mathrm{APC}}}{T_{\mathrm{PC}} + T_{\mathrm{APC}}} \times 100\% \quad (7)$$

where $T_{\mathrm{PC}} = T_{\mathrm{PC}}(E_{\mathrm{F}})_{\uparrow} + T_{\mathrm{PC}}(E_{\mathrm{F}})_{\downarrow}$, and $T_{\mathrm{APC}} = T_{\mathrm{APC}}(E_{\mathrm{F}})_{\uparrow} + T_{\mathrm{APC}}(E_{\mathrm{F}})_{\downarrow}$.

The spin-filter efficiency (SFE) with different bias voltages is defined as

$$\mathrm{BSFE} = \frac{I_{\downarrow} - I_{\uparrow}}{I_{\downarrow} + I_{\uparrow}} \times 100\% \quad (8)$$

where I_{σ} ($\sigma = \uparrow, \downarrow$, spin up: $\uparrow$; spin down: $\downarrow$) is the spin-resolved current.

The magnetoresistance ratios at different bias voltages are defined by the following two formulae[17,20]

$$\mathrm{BMR1} = \frac{I_{\mathrm{PC}} - I_{\mathrm{APC}}}{I_{\mathrm{APC}}} \times 100\% \quad (9)$$

$$\mathrm{BMR2} = \frac{I_{\mathrm{PC}} - I_{\mathrm{APC}}}{I_{\mathrm{PC}} + I_{\mathrm{APC}}} \times 100\% \quad (10)$$

where I_{PC} and I_{APC} are the total currents in the PC and the APC, respectively.

At zero bias, the charge and spin Seebeck coefficient are defined as $S_{\mathrm{C}} = (S_{\uparrow} + S_{\downarrow})/2$ and $S_{\mathrm{S}} = (S_{\uparrow} - S_{\downarrow})/2$, where $S_{\uparrow}$ and $S_{\downarrow}$ are the spin-up and spin-down Seebeck coefficients, respectively.[30]

3. Results and discussion

Fig. 2(a) and (b) show the SU and SD conductance *versus* the distance in an oscillating manner; when the distance is negative, the SU and SD conductance first increase, then decrease and then increase; the SU conductance increases and SD conductance decreases with the distance when the distance is positive in the PC. The SD conductance in the PC is larger than the one in the APC. When the distance is in the special range about −1.194 Å to −1.109 Å, the SU G is larger than the SD G (Fig. 2(c)), and when the distance is something else, the SD G is greater than the SU G. The SD and total conductance (the sum of the SU and SD conductance) reach their maximum when the distance is zero for the PC. The SU and SD conductance *versus* the distance in an oscillating manner are shown in Fig. 2(a) and (d).

Fig. 3(a) demonstrates the transmission at the Fermi level of the CuPc molecular device *versus* the distance, which is exactly the same as the change rule of the conductance. According to eqn (5), there are negative SFEs, as shown in Fig. 3(b), when the SU transmission is larger than the SD transmission in the PC and APC, and the maximum and minimum SFEs are about −26.03175% and 99.99996% for the PC, and −99.93448% and 97.91% for the APC. At zero bias, the SFE also exhibits oscillation. Fig. 3(c) and (d) show the MR ratio *versus* the distance in an oscillating manner, and the maximum MR1 and MR2 are 5.21×10^{7}% and 99.9996%, respectively. The SD G, total G and SFE of the bilayer CuPc molecular device for the PC are the greatest when the distance is zero, and the SD and total conductance for the APC are smaller than the ones for the PC. In other words, the electrical and spin properties of the bilayer CuPc molecular

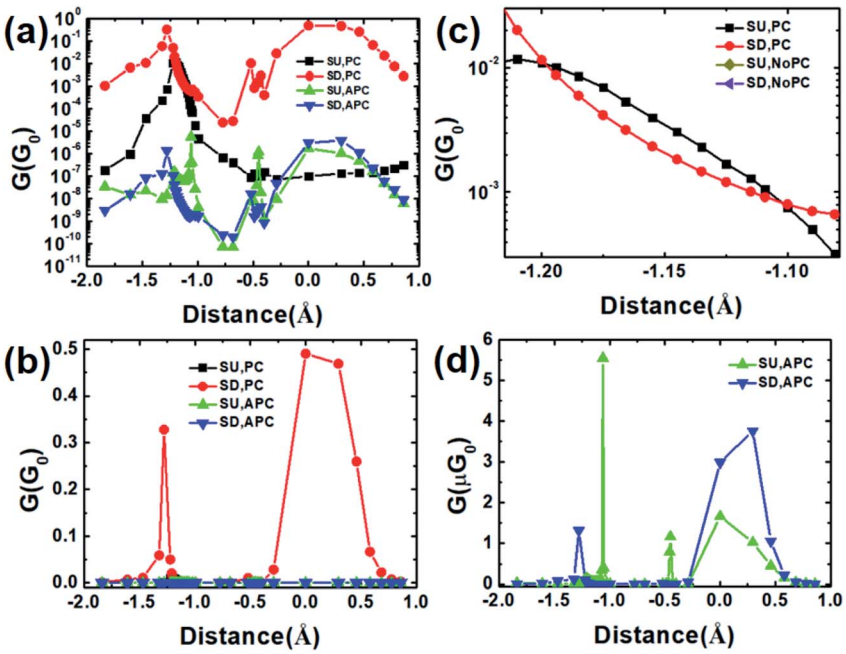

Fig. 2 At zero bias, (a and b) the SU and SD conductance G in the PC and APC and the detail in the range of −1.215 to −1.079 Å at the Fermi level of the CuPc molecular device *versus* the distance with logarithmic ordinate; (c) the SU and SD G in the PC and APC *versus* the distance with linear ordinate; (d) the SU and SD G in the APC *versus* the distance with linear ordinate.

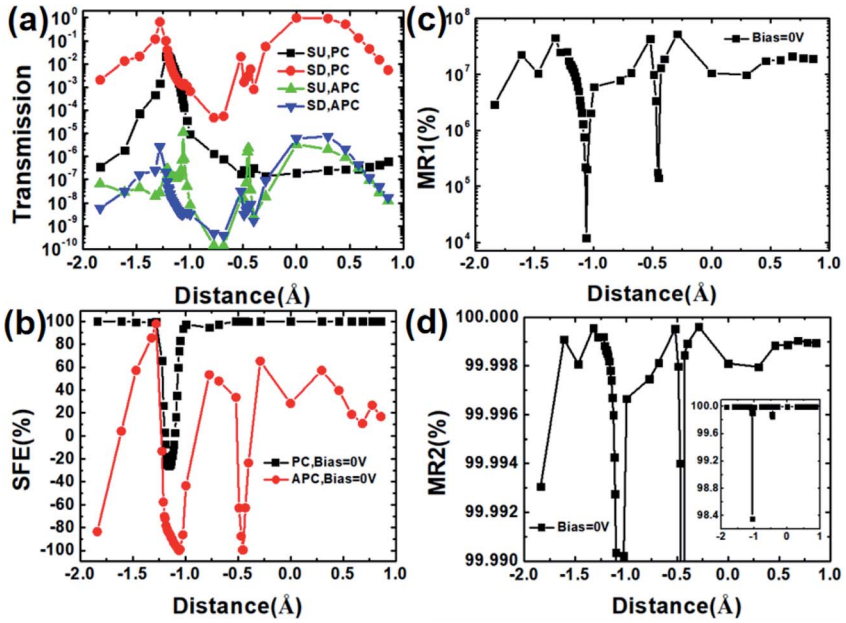

Fig. 3 (a) The spin-polarized transmission, (b) SFE and (c and d) MR ratio of the CuPc molecular device *versus* the distance.

device are optimal with $d = 0$ Å. To understand the underlying physical mechanism, we calculated the transmission spectrum, spin polarized projected (projected onto orbitals and considering the angular momentum quantum number) density of states and the scattering states, as shown in Fig. 4 and Fig. 5.

Fig. 4 demonstrates the transmission and scattering states of the CuPc molecular device in the PC with $d = 0$ Å (a–e) and $d \approx -1.16584$ Å (f–j). For the bilayer CuPc molecular device at zero bias, the transmission at the Fermi level in the SU channel is smaller than the one in the SD channel (a) and the scattering states in the SD channel are stronger than the one in the SU channel (b–e) with $d = 0$ Å (SFE $\approx$ 99.99996%). However, there is a diametrically opposite law of change for the transmission (f) and scattering states (g-j) of the device with $d \approx -1.16584$ Å (SFE $\approx -26.03175\%$).

Fig. 5 shows the transmission spectrum and the spin polarized projected (projected onto orbitals and considering the angular momentum quantum number) density of states (PDOS)

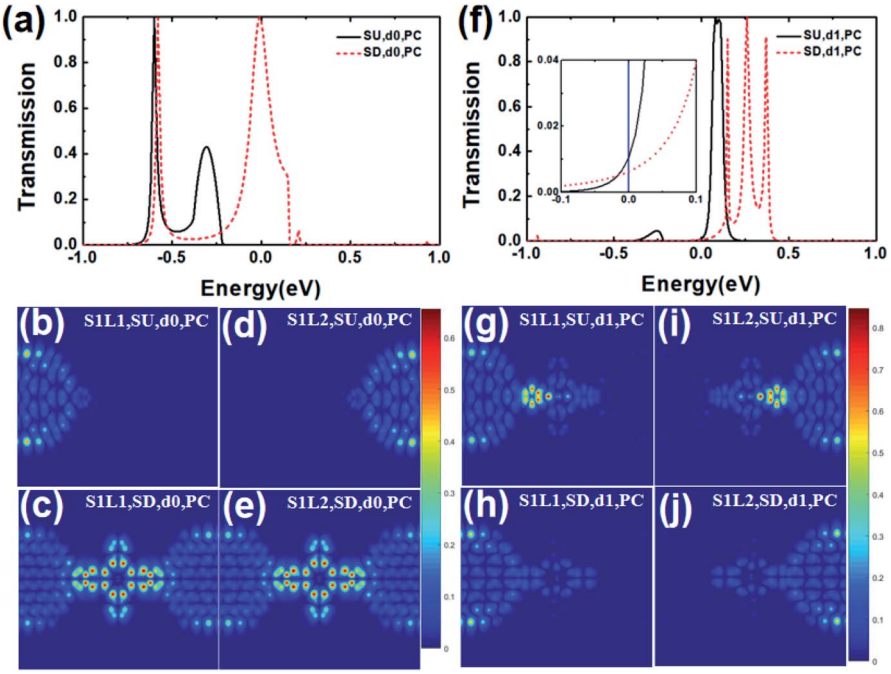

Fig. 4 The transmission and scattering states of the CuPc molecular device in the PC with $d = 0$ Å (d0) (a–e) and $d \approx -1.16584$ Å (d1) (f–j).

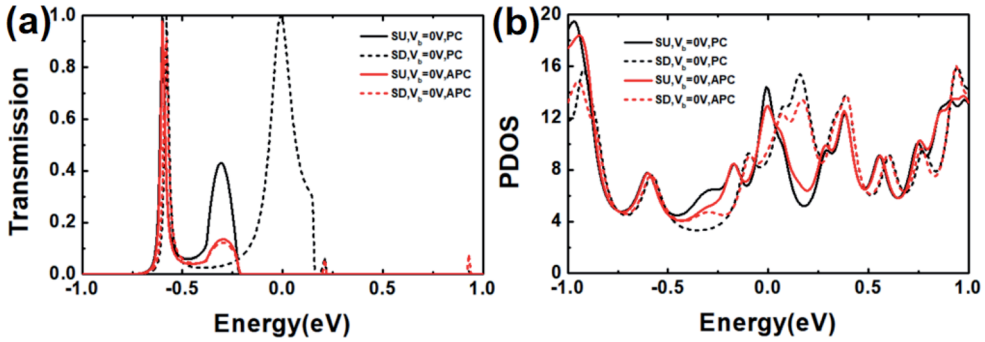

Fig. 5 The transmission spectrum and the spin polarized projected (projected onto orbitals and considering the angular momentum quantum number) density of states (PDOS) of the CuPc molecular device in the PC and APC with $V_b = 0$ V and $d = 0$ Å.

of the CuPc molecular device in the PC and APC with $V_b = 0$ V and $d = 0$ Å. The transmission spectrum for the PC is generally larger than the one for the APC. At the Fermi level, the SD transmission in the PC is clearly higher than the SU transmission and the transmission in the APC. As a whole, the PDOS in the PC is greater than the one in the APC.

The above results drove us to investigate the effect of bias voltage on the spin filtering efficiency. Fig. 6 shows the influence of bias voltage on the electrical properties of the bilayer CuPc molecular device with the distances $d = 0$ Å and $d = -1.06$ Å for the PC and APC. There is an increasing trend for the SU and SD currents when the bias increases and the bias is larger than certain values. The SD current in the PC and APC for $d = 0$ Å and the SU current in the PC and SD current in APC for $d = -1.06$ Å show a NDR effect with an onset bias of about 0.5 V. The SU current for $d = 0$ Å and SD current for $d = -1.06$ Å show a NDR effect with an onset bias of about 0.05 V and 0.2 V, respectively. The bias-dependent spin filtering efficiency (BSFE) first increases and then decreases with the PC, and first increases, then decreases and then increases with the APC with increasing considered bias voltage when $d = 0$ Å and the BSFE for $d = -1.06$ Å oscillates with increasing bias, as shown in Fig. 6(b). The largest BSFEs for $d = 0$ Å and $d = -1.06$ Å in the PC are about 99.9986% and 99.69%, and are about 99.9988% and 99.999% in the APC, respectively. The largest reversal BSFEs for $d = -1.06$ Å are about −97.08% in the PC and −85.75% in the APC. For the PC and APC, there is a giant magnetoresistance effect, and the bias-dependent magnetoresistance ratios BMR1 and BMR2 change with increasing considered bias voltage in an oscillating manner when $d = 0$ Å and $d = -1.06$ Å, as shown in Fig. 6(c) and (d). The highest MR1 values are about 1.39×10^6% and 1.97×10^4% for $d = 0$ Å and $d = -1.06$ Å, respectively. As shown in eqn (9) and (10), the SFE and MR are determined by the SU and SD currents (Fig. 6(a)).

Fig. 7 shows the transmission in the SU and SD channel of the CuPc molecular device for the PC and APC with a distance of 0 Å at $V_b = 0.01$ V and $V_b = 0.5$ V.

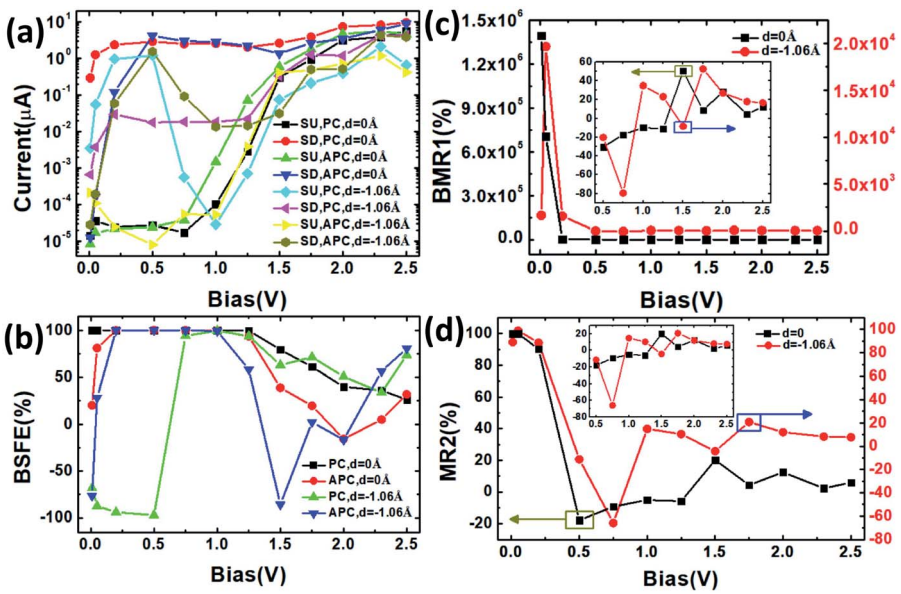

Fig. 6 (a) The spin-polarized current, (b) SFE, and (c and d) MR ratio of the CuPc molecular device *versus* the bias voltage.

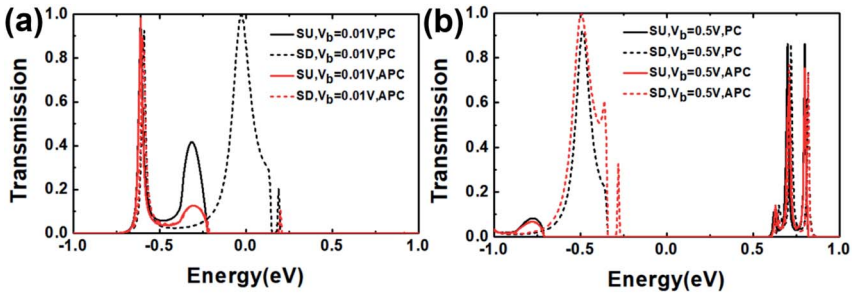

Fig. 7 The transmission spectrum of the CuPc molecular device in the PC and APC with $V_b = 0.01$ V and $V_b = 0.5$ V.

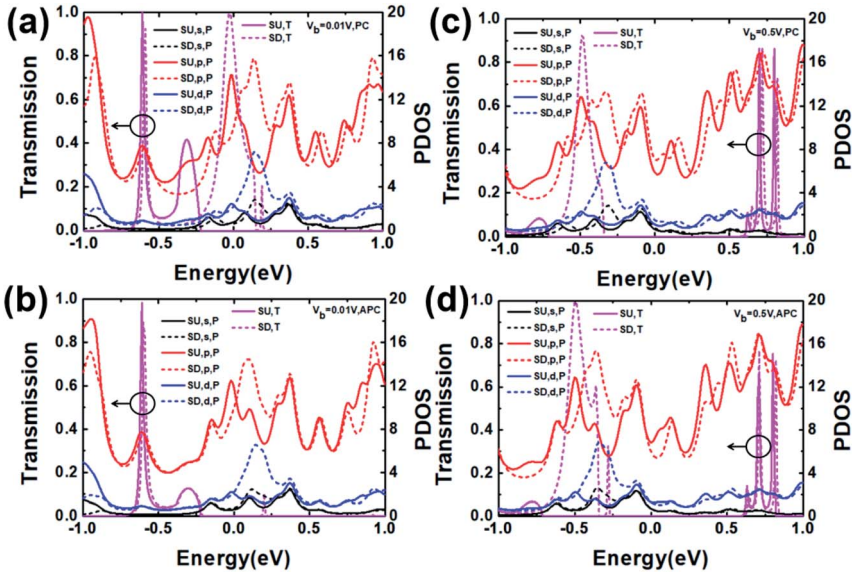

Fig. 8 The transmission spectrum and the spin polarized projected (projected onto orbitals and considering the angular momentum quantum number) density of states (PDOS) of the CuPc molecular devices in the PC and APC with $V_b = 0.01$ V in (a) and (b), and in the PC and APC $V_b = 0.5$ V in (c and d).

The SU and SD transmission for the PC at $V_b = 0.01$ V are greater than the ones for the APC (Fig. 7(a) and (b)). At $V_b = 0.5$ V, there is a little difference in the SU transmission in the PC and APC, and the SD transmission in the PC is lower than the one in the APC, as shown in Fig. 7(a) and (b), respectively. The change values of the SU and SD transmission at $V_b = 0.01$ V and $V_b = 0.5$ V correspond to the change of the spin-polarized current.

Fig. 8 shows the transmission (T) and PDOS (P) of the s, p, and d orbitals in the SU and SD channels of the CuPc molecular device for the PC and APC with a distance of 0 Å at $V_b = 0.01$ V and $V_b = 0.5$ V, which correspond to the changing rule of the spin-polarized current at bias = 0.01 V and 0.5 V.

At bias = 0.01 V, as shown in Fig. 8(a), there are two main transmission peaks from −1 eV to 1 eV: about −0.59 eV and −0.025 eV for SD, and about −0.61 eV and −0.31 eV for SU for the PC. There is one main transmission peak for the SU and SD channel (Fig. 8(b)) at about −0.61 eV and −0.59 eV, respectively. At bias = 0.5 V, as shown in Fig. 8(c) and (d), there are two main transmission peaks of about 0.7 eV and 0.8 eV for the SU channel and three main transmission peaks of about −0.49 eV, 0.71 eV and 0.81 eV for the SD channel for the PC. For APC, there are two main transmission peaks of about 0.7 eV and 0.8 eV for the SU channel and four main transmission peaks of −0.49 eV, −0.36 eV, 0.71 eV and 0.82 eV for the SD channel (Fig. 8(d)). The origin of the transmission peaks could be figured out by

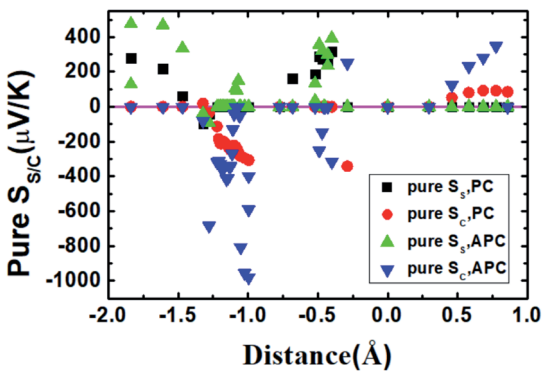

Fig. 9 The pure spin Seebeck coefficient and charge Seebeck coefficient of the CuPc molecular device in the PC and APC *versus* the distance.

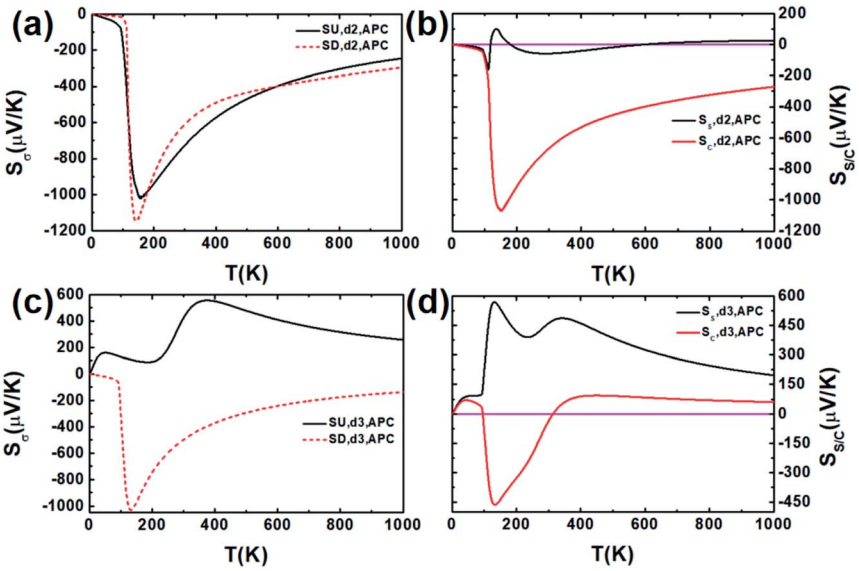

Fig. 10 The spin-dependent Seebeck coefficient S_σ, the spin Seebeck coefficient S_S and the charge Seebeck coefficient S_C of the CuPc molecular device in the APC *versus* temperature for distances of about −0.9958 Å (d2) in (a) and (b), and for distances of about −1.8388 Å (d3) in (c) and (d).

projected density of states (PDOS);[12] therefore, we demonstrated the PDOS of the s, p, d orbitals in the SU and SD channels of the CuPc molecular device with the PC and APC (Fig. 8). As shown in Fig. 8(a–d), the transmission is mainly controlled by the PDOS of the p orbital. The transmission peaks essentially coincide with the corresponding PDOS peaks, and most other PDOS peaks have no distribution to the transmission peaks.

Fig. 9 shows the pure spin Seebeck coefficient ($S_C = 0$) and charge Seebeck coefficient ($S_S = 0$) of the CuPc molecular device in the PC and APC *versus* the distance. It can be seen that when the distance is greater than about 0.5 Å, there is only the pure charge Seebeck coefficient in the PC and APC, that is, there is a pure charge flow at the corresponding temperature difference. As the distance increases, the pure charge Seebeck coefficient first increases and then decreases in the PC, while the pure charge Seebeck coefficient in APC increases, that is, the corresponding pure charge flow increases. However, when the distance is about 0.859 Å, the pure S_S and S_C are zero, that is, there are no pure S_S and S_C at the corresponding temperature. When the distance is negative, in different regions, there are pure spin Seebeck coefficients and pure charge Seebeck coefficients for the PC and APC, respectively, that is, there are pure spin current and pure charge current. When the distance is around −0.5 Å, there is a positive pure spin Seebeck coefficient for the PC and APC, and there is a negative pure charge Seebeck coefficient for the APC. When the distance is near 1 Å, there is a large negative pure charge Seebeck coefficient; when the distance is less than about −1.46 Å, there is a positive pure spin Seebeck coefficient for the PC and APC, and it increases with decreasing distance, that is, there is a pure spin current increasing with decreasing distance. As shown in Fig. 10(b) and (d), when the distances are about −0.9958 Å (d2) and −1.8388 Å (d3), there are three pure S_C and two pure S_S at different temperatures in the APC, respectively, which means that there are three and two different temperature differences to produce pure charge current and pure spin current, respectively. Fig. 10(a) shows that the SU and SD Seebeck coefficients first decrease and then increase with the temperature; the SD Seebeck coefficient first decreases and then increases with the temperature; however, the SU Seebeck coefficient first increases, then decreases, then increases and then decreases with temperature.

4. Conclusions

In conclusion, we have investigated the spin-dependent conductance, current, SFE and MR ratio of a bilayer CuPc molecular device with different buffer layer-molecule distances using DFT-NEGF. The results show that the greatest spin filter efficiency of the bilayer CuPc molecular device at zero bias exceeds 99.99996% in the parallel spin configuration and 97.91% in the anti-parallel spin configuration. Particularly, there are reserved SFEs for the PC and APC when the distances are certain values, and the reserved SFEs exceed −26.03175% and −99.93448%, respectively. For the PC and APC, there is a giant magnetoresistance effect, and the MR ratio exceeds 5.21×10^7% (99.9996%). Moreover, the MR is reserved when the bias voltage is at certain values. With an applied bias, a negative differential resistance effect was observed for the distance at certain values, such as $d = 0$ and −1.06 Å. When the distances are certain values, there are pure spin Seebeck coefficients and pure charge Seebeck coefficients at certain temperatures, which means that the corresponding temperature differences could produce pure spin current and pure charge current. Our results provide a promising approach for designing high-performance spintronic and spin thermoelectric molecular devices.

Conflicts of interest

There are no conflicts to declare.

Acknowledgements

This work was supported by the National Key Research and Development Program of China under Grant No. 2021YFA1200502, the General Program of National Natural Science Foundation of China under Grant No. 12174423 and 61774168.

References

1 S. A. Wolf, D. D. Awschalom, R. A. Buhrman, J. A. Daughton, S. von Molnár, M. L. Roukes, A. Y. Chtchelkanova and D. M. Treger, *Science*, 2001, **294**, 1488.
2 S. Lakshmi, S. Roche and G. Cuniberti, *Phys. Rev. B*, 2009, **80**, 193404.
3 J. Huang, W. Y. Wang, Q. X. Li and J. L. Yang, *J. Chem. Phys.*, 2014, **140**, 164703.
4 H. Hao, X. H. Zheng, Z. X. Dai and Z. Zeng, *Appl. Phys. Lett.*, 2010, **96**, 192112.
5 S. Schmaus, A. Bagrets, Y. Nahas, T. K. Yamada, A. Bork, M. Bowen, E. Beaurepaire, F. Evers and W. Wulfhekel, *Nat. Nanotechnol.*, 2011, **6**, 185–189.
6 A. R. Rocha, V. M. Garcia-Suárez, S. W. Bailey, C. J. Lambert, J. Ferrer and S. Sanvito, *Nat. Mater.*, 2005, **4**, 335.
7 N. Atodiresei, J. Brede, P. Lazic, V. Caciuc, G. Hoffmann, R. Wiesendanger and S. Blugel, *Phys. Rev. Lett.*, 2010, **105**, 066601.
8 H. Wan, B. Zhou, X. Chen, C. Q. Sun and G. Zhou, *J. Phys. Chem. C*, 2012, **116**, 2570.
9 X. Q. Deng, Z. H. Zhang, G. P. Tang, Z. Q. Fang, L. Sun and C. X. Li, *Org. Electron.*, 2016, **35**, 1.
10 T. Tada, S. Hamayama, M. Kondo and K. Yoshizawa, *J. Phys. Chem. B*, 2005, **109**, 12443.
11 Y. F. Wang, J. Kroger, R. Berndt and W. A. Hofer, *J. Am. Chem. Soc.*, 2009, **131**, 3639.
12 C. C. Zhao, S. H. Tan, X. F. Peng, X. J. Wang and M. Q. Long, *Org. Electron.*, 2017, **43**, 47–54.
13 C. Arrigo, F. Andrea and N. M. Buongiorno, *Nanotech*, 2007, **18**, 15464.
14 J. Zeng and K. Q. Chen, *J. Mater. Chem. C*, 2013, **1**, 4014.
15 Y. D. He, H. L. Dong, T. Li, C. L. Wang, W. Shao, Y. J. Zhang, L. Jiang and W. P. Hu, *Appl. Phys. Lett.*, 2010, **97**, 133301.
16 J. Huang, K. Xu, S. Lei, H. Su and S. Yang, *J. Chem. Phys.*, 2012, **136**, 064707.
17 L. L. Tao and J. Wang, *Nanoscale*, 2017, **9**, 12684–12689.
18 D. Waldron, P. Haney, B. Larade, A. MacDonald and H. Guo, *Phys. Rev. Lett.*, 2006, **96**, 166804.
19 B. Wang, J. W. Li, Y. J. Yu, Y. D. Wei, J. Wang and H. Guo, *Nanoscale*, 2016, **8**, 3432–3438.
20 X. X. Han, J. J. Yang, P. P. Yuan and B. A. Bian, *Eur. Phys. J. B*, 2019, **92**, 32.
21 X. X. Fu, F. Wei, Y. Niu and C. K. Wang, *Phys. E*, 2021, **131**, 114737.
22 J. H. Liu, K. Luo, K. L. Huang, B. Sun, S. L. Zhang and Z. H. Wu, *Nanoscale Adv.*, 2021, **3**, 3497–3501.
23 Z. H. Wu, L. Z. Lin, W. Yang, D. Zhang, C. Shen, W. Lou, H. Yin and K. Chang, *RSC Adv.*, 2017, **7**, 30963–30969.
24 P. Hohenberg and W. Kohn, *Phys. Rev.*, 1964, **136**, 864–871.
25 W. Kohn and L. J. Sham, *Phys. Rev.*, 1965, **140**, 1133–1138.
26 J. Taylor, H. Guo and J. Wang, *Phys. Rev. B*, 2001, **63**, 245407.
27 L. L. Cui, B. C. Yang, X. M. Li, J. He and M. Q. Long, *Int. J. Mod. Phys. B*, 2014, **28**, 1450019.
28 M. Buttiker, Y. Imry, R. Landauer and S. Pinhas, *Phys. Rev. B*, 1985, **31**, 6207–6215.
29 N. A. Bruque, M. K. Ashraf, G. J. O. Beran, T. R. Helander and R. K. Lake, *Phys. Rev. B*, 2009, **80**, 155455.
30 M. X. Zhai, X. F. Wang, P. Vasilopoulos, Y. S. Liu, Y. J. Dong, L. P. Zhou, Y. J. Jiang and W. L. You, *Nanoscale*, 2014, **6**, 11121–11129.